Progress In Electromagnetics Research C, Vol. 137, 93–109, 2023

Miniaturized Hexagonal Antenna with Defected Ground Plane for 5G MM Wave Applications

Ramya Shetty[1], Ashish Singh[1, 2, *], Anil K. Bhat[1], Satheesh Rao[1], and Harshitha Bhat[1]

Abstract—The paper presents a very compact hexagonal millimeter wave antenna of dimension $9 \times 5 \times 0.25\,\text{mm}^3$ with defected ground plane for mm-wave applications. The parametric design analysis is done for circular patch and hexagonal antenna on the same defected ground plane, and performance parameters of the antenna are analyzed. The designed hexagonal antenna with defected ground plane is compared with existing planar mm antennas in literature and works in ultra-wideband frequency at 40 GHz to 52 GHz with a minimum gain of 5.3 dBi and maximum gain of 6.5 dBi over the band and has the total efficiency of 80–95.9%. Antenna characteristic behavior is analyzed by varying the length of notches of the ground plane and other parameters such as thickness of the substrate, dielectric constant, and width of the strip of antenna. The antenna equivalent model is presented and is also simulated using Linear Technology (LT Spice). The radiation patterns are analyzed, and S_{11} impedance of the antenna is studied using the Smith chart. The antenna is simulated using CST Microwave Studio simulation tool and fabricated, and the results are validated using VNA (Vector Network Analyzer). This antenna's low profile enables easy integration with micro-circuits and can be used in applications such as fixed and mobile satellite, earth explorations satellite, space research services, broadcasting satellite services, international mobile telecommunication services, and High-Altitude Platform Systems (HAPS) services in mm-wave domain.

1. INTRODUCTION

In recent times for data communication, there is a requirement of high data rates in gigabits/second and terabits/second for majority of the applications. These applications such as video transfer over internet, gaming applications over internet, video conferencing, vehicular communication, internet over mobile, also the advancement of multimedia technology have resulted in researches in mm-wave range. The mm-wave spectrum is capable of offering high data rates as 5% relative bandwidth at 60 GHz Industrial Scientific and Medical (ISM) band is 3 GHz of bandwidth as compared to 2.4 GHz ISM band which is only 120 MHz bandwidth [1]. This has motivated most researchers to shift from non mm-wave range, (450 MHz–7.125 GHz) (FR1 — Frequency Range1) to mm-wave range FR2 (24.25 GHz–52.6 GHz) range [1]. The Verizon American Business Company is working with FR2 band and has set up a 5G network on mm-wave band and is already providing 5G services in 30 cities in America. Samsung is another leading service provider which has developed a technology operating in millimeter wave for Ka band in wireless communication [2]. The World Radiocommunication Conference (WRC) 40 GHz band includes applications such as fixed and mobile satellite (space to earth), earth explorations satellite, space research satellite services, broadcasting satellite services, radio astronomy and High altitude Platform

Received 29 May 2023, Accepted 17 August 2023, Scheduled 30 August 2023
* Corresponding author: Ashish Singh (ashsin09@rediffmail.com).
[1] Department of Electronics & Communication Engineering, Visvesvaraya Technological University (VTU), Belagavi 590018, Karnataka, India. [2] Department of Computer & Communication Engineering, NMAM Institute of Technology, Nitte-574110, Affiliated to NITTE (Deemed to be University), Karnataka, India.

stations frequency assignment services [3, 4]. The WRC 50 GHz band includes applications such as fixed non geostationary satellites, international mobile telecommunication services, and HAPS services [3, 4].

Since mm-wave spectrum has lots of significance, there is much scope for research in this field, authors have investigated the current trend and developments in mm-wave antennas and also discussed different fabrication technologies of mm-wave antennas [5]. Further, some authors have compared the propagation characteristics of different mm-wave frequency bands such as 11 GHz, 16 GHz, 28 GHz, and 38 GHz [6]. Thereafter, a leaky wave antenna with a compact microstrip line working in frequencies 35 GHz to 41.5 GHz has been discussed [7]. Subsequently, an ultra-wideband phase shifter with frequency ranges 24 GHz–30 GHz and 37 GHz–43.5 GHz is discussed to meet multiband requirements of 5G millimeter wave [8]. Later, a few articles in which channel measurements of mm-wave Multiple-Input Multiple-Output (MIMO) antennas of 4×4 at 28 GHz, 32 GHz, and 38 GHz are presented [9]. Moreover, some authors have discussed the necessity of huge data rate such as gigabits/second or terabits/second which tells the importance of mm-wave communication and terahertz communication [10]. Also, a log periodic antenna with ultra-wideband of 25 GHz to 35.5 GHz is developed [11]. Some authors have reported a new way of designing mobile communication using 28 GHz and 39 GHz millimeter wave frequency bands with semiconductor technologies at mm-wave band [12]. Further, a new type of 3D integration and 3D interconnection techniques have been developed for mm-wave system design [13]. Hereafter, an antenna is developed for Ka/V dual bands for body centric network applications with frequencies 33.5 GHz and 60.8 GHz operating in Ka and V bands, respectively [14]. In addition, a MIMO small sized antenna which offers ultra-wideband operation from 25 GHz to 50 GHz has been presented [15].

Some of the literatures also report antennas with defected ground plane. The simple antennas for mobile phones using 5G with millimeter wave bands at (26.75 to 30.31) GHz and (35.83–41.22) GHz with shortened ground plane are presented [16]. An antenna is studied where the effect of finite and optimized ground plane is considered for mm-wave applications [17]. Then a small stripfed dual band antenna with a small slot in the partial ground for better impedance matching for mm-wave applications has been discussed [18]. Additionally, an adaptive tri-band antenna is considered for mm-wave band [19]. Moreover, a dual band slot antenna is reported with an elliptical opening in the ground plane for 28 GHz to 38 GHz [20]. Besides these, an antenna for 38 GHz frequency with microstrip feed is designed which enables easy integration [21]. Also, an antenna which radiates in all directions is reported for 38 GHz frequency with a notch in the incomplete ground [22]. Furthermore, a cavity backed antenna is presented for 37.5 GHz and 42 GHz frequencies [23]. Thereafter, an array antenna for 40/50 GHz is discussed with a parasitic cell in the bottom layer [24]. Thus, it is observed from literature that antennas resonate at

Table 1. Proposed antenna with other mm and planar antennas present in literature.

Ref.	Resonant Frequency	Bandwidth (GHz) (%)	Gain (dB)	Radiation Efficiency (%)	Size ($mm^{3)}$
[16]	38.0	13.9	4.50	80.0	$6.0 \times 8.0 \times 0.250$
[17]	38.50	11.9	2.90	90.0	$30.0 \times 15.0 \times 0.2540$
[18]	38.0	16.9	9.494	89.0	$55 \times 110 \times 0.508$
[19]	38.0/48.0	11.5 8.5	8.390 7.730	81.0/83.0	$34.80 \times 34.80 \times 0.5080$
[20]	38.0	28.5	6.90	80.0	$8 \times 7.5 \times 0.127$
[21]	38.0	13	-	68.80	$15.6 \times 13 \times 0.254$
[22]	38.0	7.8	1.830	78.0/76.0	$14.0 \times 12.0 \times 0.380$
[23]	47.5	2.8	5.70	-	$15.40 \times 8.0 \times 0.5080$
[24]	40.0/50.0	22	7.3/12.5	-	$17.70 \times 10.0 \times 0.5080$
Proposed work	42.0	26	6.0	95.9	$9 \times 5 \times 0.25$

mm-wave frequency, if defects are present in the ground plane.

Authors have reported a MIMO Hexagonal antenna for an Ultra-Wideband (UWB) range of 2.1 to 11.4 GHz [25]. Vahid Sarani and Neshati reported a hybrid antenna using partial-hexagonal cavity [26]. The antennas presented in literature are compared with proposed antennas listed in Table 1. Further, it is observed from the table that there are still opportunities for improvement of antenna characteristics and size.

In terms of size constraint antenna has been designed to achieve optimal gain and efficiency in comparison with previous proposed antennas. In this view, a hexagon-shaped patch antenna with defected ground for mm-wave application is proposed.

In this manuscript a simple, small, hexagonal antenna working for mm-wave range is designed which can be easily embedded in small devices and can also be used for vehicular communication as it can provide higher data rate.

2. ANTENNA DESIGN AND FABRICATION

The antenna is constructed with a defected ground plane having the initial length and width of ground plane $L \times W$ mm^2 with three notches having dimensions as shown in Table 2. The notches are sliced from the ground plane to create a defect in the ground radiating structure as shown in Fig. 1. The Hexagonal Patch Antenna (HPA) has been simulated using Computer Simulation Technology (CST) studio suite, and the computational method used for simulation is Finite Integration Technique (FIT).

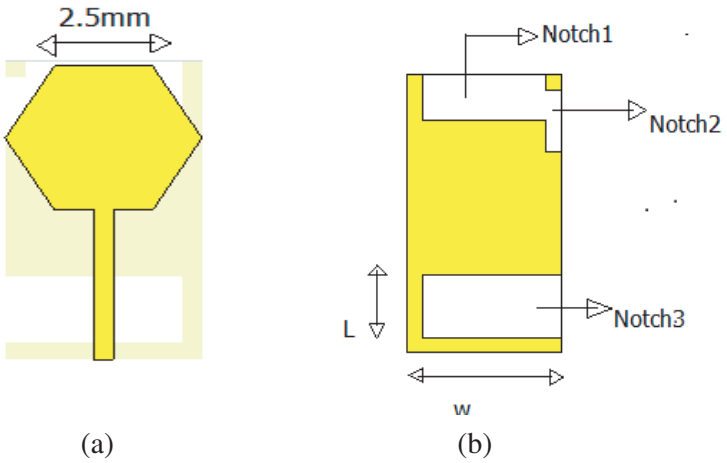

Figure 1. Hexagonal antenna. (a) Front view. (b) Back view.

Table 2. Notch dimensions.

S. No.	Notches	Length (mm)	Width (mm)
1	Notch1	1.5	4
2	Notch2	2	0.5
3	Notch3	2	4.5

A notch1 of 1.5 mm × 4 mm, a notch2 of 2 mm × 0.5 mm, and a notch3 of 2.00 mm × 4.5 mm are sliced at the top of the radiating side, along the width side, and from the feed side of the patch from the ground plane, respectively. The same ground plane shown in Fig. 2(a) is used for all patches simulated shown in Fig. 2.

The antenna shown in Fig. 3 is designed on an FR4-Flame Retardant4 substrate of 0.25 mm thickness with a permittivity of 4.3 having a small dimension of $9 \times 5 \times 0.25$ mm^3. The antenna is

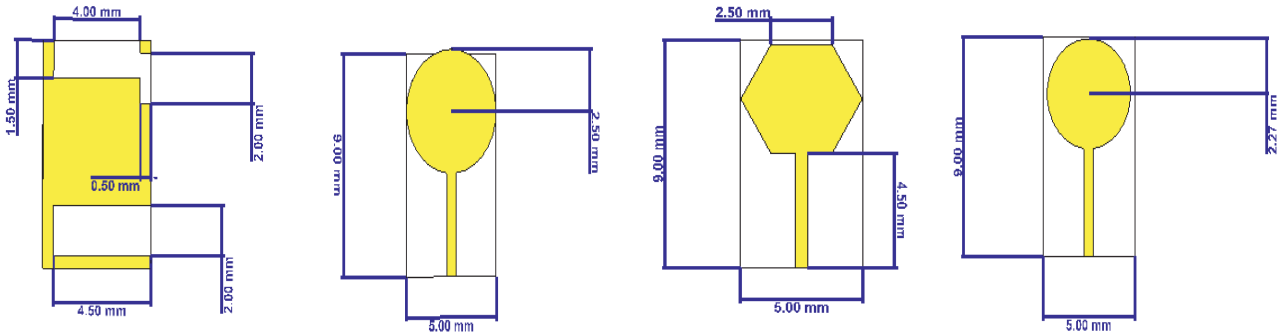

Figure 2. Dimensions of ground, circle with radius 2.5 mm, hexagon with side 2.5 mm and circle with radius 2.27 mm. (a) Ground view. (b) Circular patch ($R = 2.5$ mm). (c) Hexagonal patch ($S = 2.5$ mm). (d) Circular patch ($R = 2.27$ mm).

Figure 3. Hexagonal antenna of dimension 9 mm × 5 mm. Top and Back view.

applicable where optimization of the area is required. The antenna is fabricated using Chemical Vapor Deposition (CVD) technique. It deals with the area of broad thin film deposition technique used for producing elevated quality solids. CVD process involves gaseous chemical reaction followed by heat or plasma to produce thin films on a substrate. It results in solids with an even thickness.

SubMiniature-A (SMA) connector has been used to excite the antenna shown in Fig. 3, and the subminiature connector of range 2.9 mm is used for connecting.

3. PARAMETRIC DESIGN ANALYSIS

A circular patch is designed for resonance at 38 GHz for operation in n260 band (37 GHz–40 GHz). An FR4 substrate having a dielectric constant of 4.3 and thickness of 0.252 mm is used. Using Equation (1) from [27], dimension of the patch for different modes of operation is calculated and given in Table 3.

$$fo = \frac{K_{nm}c}{2\pi a_e\sqrt{\in_r}} \tag{1}$$

Table 3. [27].

Mode (n, m)	Root (K_{nm})
1, 1	1.84118
2, 1	3.05424
3, 1	4.20119

The effective radius is calculated for modes mentioned in the Table 3 for 38 GHz. The obtained values of the effective radius a_e are 1.11 mm, 1.85 mm, and 2.55 mm for $K_{nm} = 1.84118$, $K_{nm} = 3.05424$, and $K_{nm} = 4.20119$, respectively. A 50 Ω feed line at 38 GHz has to have a minimum width of 0.5 mm which is calculated using Equations (2) and (3) [27].

$$\in_{eff} = \frac{\in_r +1}{2} + \frac{\in_r -1}{2}\left(1 + \frac{10h}{w}\right)^{-\frac{1}{2}}; \quad \frac{w}{h} \gg 1 \tag{2}$$

$$Z_o = 376.6/(\sqrt{(\in\_eff)}(w/h + 1.4 + 0.667\ln(w/h + 1.444))\,\text{ohm}; \quad \frac{w}{h} > 1 \tag{3}$$

Since good sizing ratio was required for fabrication TM_{31} was chosen, and the patch was designed to have a radius of 2.5 mm to account for the fringing fields. The designed antenna structure was simulated and found to resonate at 41.34 GHz. The hexagonal patch is designed by using the same circular patch by dividing the circumference of the circular patch with radius 2.5 mm into 6 segments. The hexagonal patch has each segment measuring 2.5 mm. The resonant frequency of the hexagonal element is calculated using Equation (4) [27] which turns out to be 42 GHz where K_{nm} is defined in Table 1. The hexagonal patch having edge dimension S of 2.5 mm when simulated resonates at 42 GHz.

$$f_r = \frac{K_{nm}c}{2\pi\,(0.9094S)\,\sqrt{\in_r}} = \frac{1.1K_{nm}c}{2\pi S\sqrt{\in_r}} \tag{4}$$

$$a_{eq} = 0.9094S \tag{5}$$

The equivalent radius a_{eq} is determined using Equation (5) [27] and found to be 2.27 mm. The simulated results of different patches are compared. The circular patch with radius 2.5 mm, hexagon with side 2.5 mm, circle with radius 2.27 mm resonate at 41.48 GHz, 42 GHz, and 41.772 GHz, respectively. The resonant frequency of the hexagonal patch slightly shifts towards the higher end from that of the circular patch with radius 2.5 mm due to drop in the effective area shown in Fig. 4. The circle with radius 2.27 mm simulated resonates at 41.772 GHz.

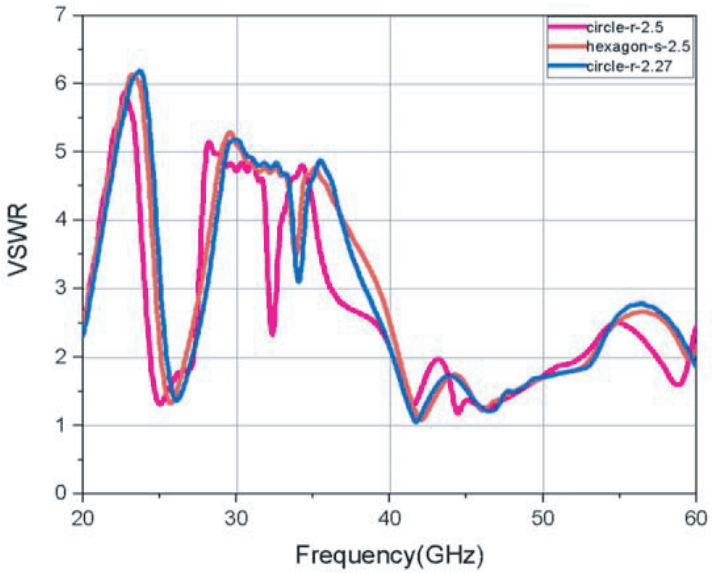

Figure 4. VSWR plot for circle with radius 2.5, hexagon with side 2.5 and circle with radius 2.27.

The Voltage Standing Wave Ratio (VSWR) and Gain plots of circle with radius 2.5 mm, hexagon with side 2.5 mm, and circle with 2.27 mm are shown in the Fig. 4 and Fig. 5. The resonant frequency, percentage bandwidth, efficiency, and gains are tabulated in Table 4.

Comparing the results of circle with radius 2.5 mm, hexagon with side 2.5 mm, and circle with radius 2.27 mm, the hexagonal antenna is considered for further parametric analysis.

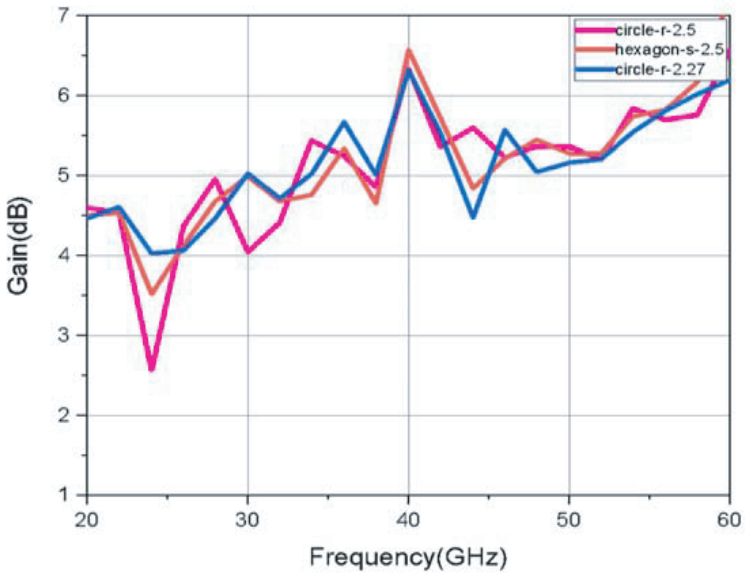

Figure 5. Gain variation for circle with radius 2.5, hexagon with side 2.5 and circle with radius 2.27.

Table 4. Simulated performance parameters of circle r — 2.5 mm, hexagon-s — 2.5, and circle-r — 2.27.

S. No.	Resonant frequency (GHz)	Bandwidth (%)	Resonant Band (GHz)	Total Efficiency over the band (dB) (%)	Average Gain over the band (dBi)
Circle radius — 2.5 mm	41.48	6.4	40.3–43	84–92	5.1–6.3
Hexagon-side — 2.5 mm	42.019	26.086	40–52	80–95.9	5.3–6.5
Circle radius — 2.27 mm	41.77	26.086	40–52	84.2–95.9	5.2–6.3

***Variation of Length of the Ground plane*:** The lengths of notch1, notch2, and notch3 of the ground are varied, and some of the best results are tabulated as shown in Table 5.

The ground plane with top 4 best results is shown in Fig. 6.

Figures 6(a), 6(b), 6(c), and 6(d) correspond to serial numbers 1, 2, 3, and 4 in Table 5, respectively.

It is observed from Table 5 that ground plane with notch1 dimension 1.5 mm × 4.5 mm, notch2 dimension 2 mm × 0.5 mm, and notch3 dimension 2 mm × 4.5 mm corresponding to serial number 1 from Table 5 gives optimum results and can be fabricated with ease compared to others with smaller notch dimensions, resulting in resonance at 42 GHz, bandwidth of 26%, total efficiency of the antenna over the band of 80–95.9%, and average gain over the band 5.3–6.5 dBi. The simulated VSWR is shown in Fig. 7 for the Hexagonal antenna (Fig. 2(c)) designed having a ground plane (Fig. 2(a)).

Keeping ground plane the same, the dimension of patch, permittivity of the substrate, substrate thickness, and strip width are varied for hexagonal patch antennas shown in Figs. 8(a), 8(b), 8(c), and 8(d), respectively.

The radius of the hexagonal microstrip antenna is varied from 2.5 mm to 1 mm shown in Fig. 8(a). It is observed from the VSWR graphs of Fig. 8(a) that there is a shift in resonant frequency towards the higher side. This is because as the effective area of radiation for patch is reduced the frequencies shift towards the higher side.

Similarly, if the permittivity of the substrate of the hexagonal microstrip antenna is varied keeping

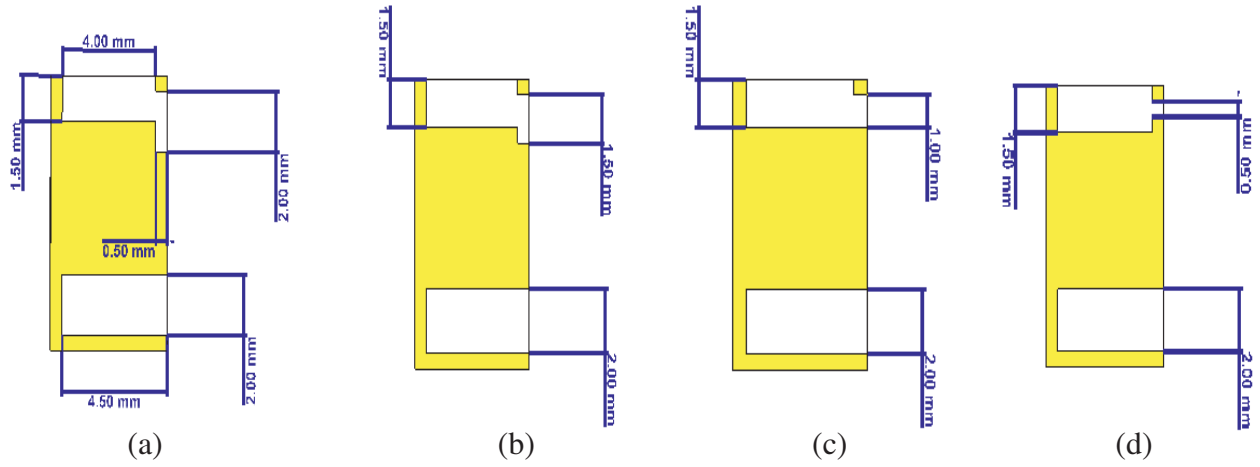

Figure 6. Ground plane variation along length.

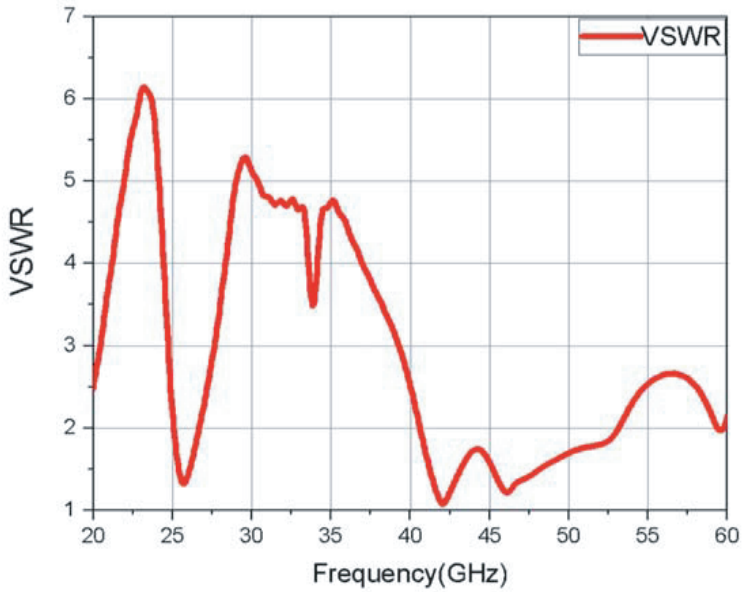

Figure 7. VSWR plot for Hexagonal patch antenna of side 2.5 mm.

the values of other parameters constant shown in Fig. 8(b), it is observed from VSWR graphs of Fig. 8(b) that bandwidth increases with decrease in permittivity of the substrate and the bandwidth obtained from dielectric constant as air with $\varepsilon_r = 1$ is the highest.

If the thickness of the substrate for hexagonal microstrip antenna is varied for standard heights of substrate keeping other parameters constant, then it is observed from the VSWR graphs of Fig. 8(c) that resonant frequency shifts towards the higher side.

As the width of the microstrip line increases by 0.1 mm, shown in Fig. 8(d), VSWR values increase towards a higher value. It is noticed from Fig. 8(d) that for a width of 0.8 mm the VSWR is greater than 2 as compared to original strip width of the line which is 0.5 mm. There is shift in resonance towards the higher frequency. Also, the total efficiency of the antenna changes as the strip width is decreased or increased from 0.5 mm. The total efficiency of the antenna at width 0.5 mm for center frequency (46 GHz) decreases from 96.4% to 91.3% at width 0.8 mm and to 82% at width 0.1 mm.

Table 5. Simulated Performance parameters for variation of slot length.

S. No.	Notch_L1 (mm)	Notch_L2 (mm)	Notch_L3 (mm)	Resonant Frequency (GHz)	Resonant Band (GHz)	Bandwidth (%)	Efficiency (%) Over the Band	Gain (dBi) Over the Band
1	**1.5**	**2**	**2**	**42.08**	**40.737–52.912**	**26.0**	**80–95.9**	**5.3–6.5**
2	1.5	1.5	2	42.3	40.869–53.139	26.104	80–95.9	5.1–6.4
3	1.5	1	2	42.291	40.815–53.125	26.2	80–95.9	5.4–6.5
4	1.5	0.5	2	41.956	40.513–53.033	26.76	80–95.9	5.5–6.5
5	1	1	2	44.55	41.787–51.165	20.1	89–95.9	5.1–5.8
6	1	1.5	2	44.626	42.164–51.206	19.4	89–95.9	5–5.7
7	0.5	2	2	43.362	41.663–50.595	19.3	70–95.9	4.9–6.2
8	0.5	1.5	2	43.515	41.575–50.537	19.4	79–95.9	5.0–6.5
9	0.5	1	2	43.359	41.598–50.513	19.3	79–100	5.0–6.5
10	0.5	0.5	2	43.265	41.641–50.355	18.9	70–100	5.1–6.3
11	0	1.5	2	42.494	41.194–49.476	18.2	79–85	4.6–5.9

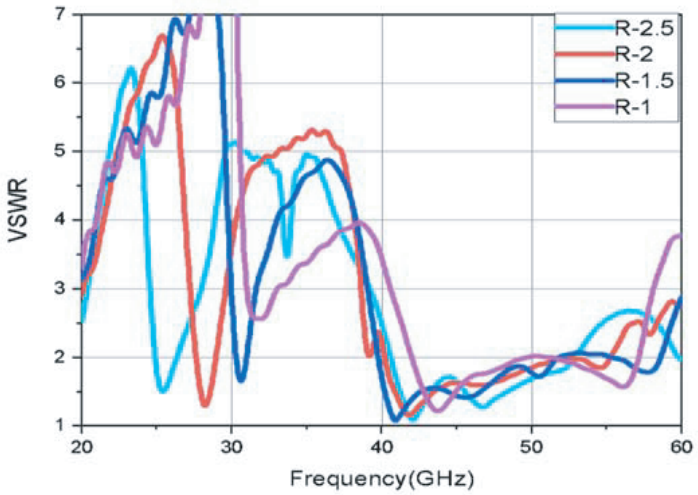

(a)

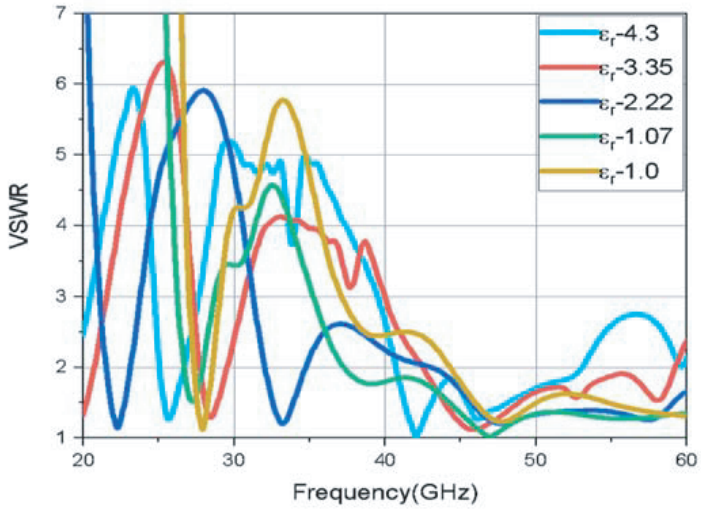

(b)

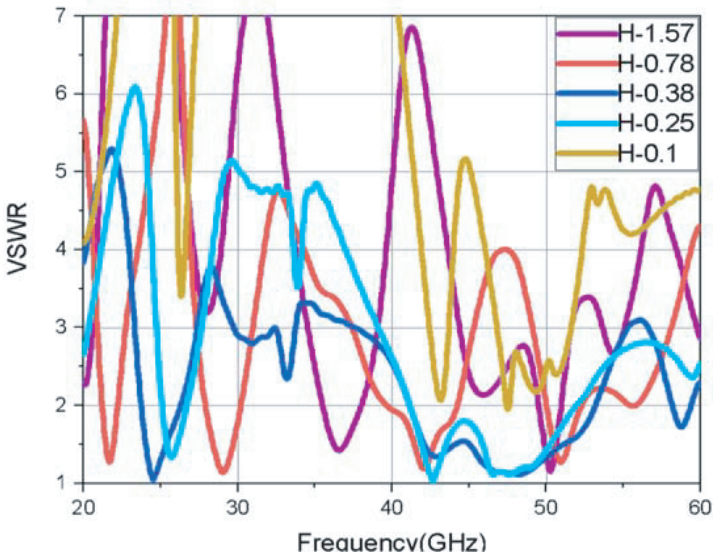

(c)

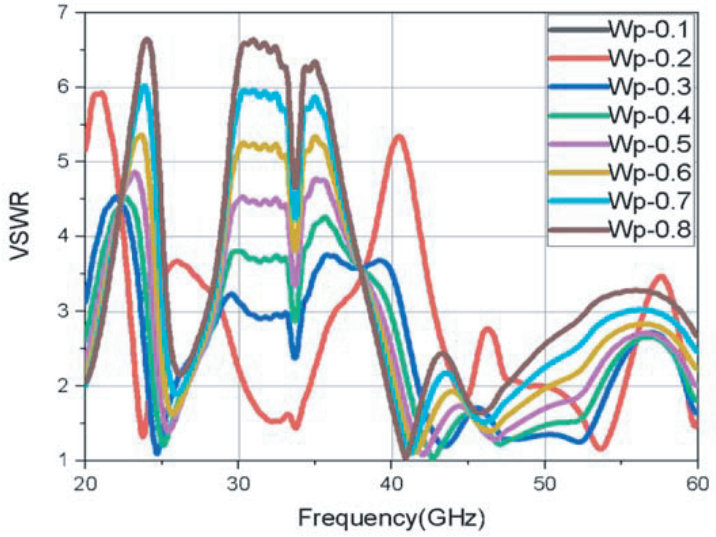

(d)

Figure 8. (a) Variation of dimension of proposed patch. (b) Variation of dielectric constant proposed hexagonal patch. (c) Variation of substrate thickness. (d) Variation of strip width of Hexagonal patch.

4. EQUIVALENT CIRCUIT

The proposed HPA can be represented into its equivalent circuit model considering Fig. 9 for creating its equivalent diagram. The HPA can be considered as a corner curtailed rectangular patch [28]. The impedances of feed and of the conventional patch are modeled by Z_{feed} and Z_{patch}. Mutual coupling capacitance between the ground and the patch is modeled as C_c. The triangular cuts etched from patch modeled as C_{def} and resistance for the triangular cuts from the patch as Z_o. The defected ground plane is modeled as Z_{defG}. The circuit model is shown in Fig. 10(a). The 3 slots in the ground plane are resonator circuits. The impedance Z_{patch} includes R_p, L_P, and C_p where the circuit parameters such as R_p, L_p, and C_p are calculated using Equations (6), (7), (8), and (9) [27]. The equation for S is calculated using Equation (10). The equation for C_{def} is given in Equation (11) [28].

$$R_p = Q/\omega_O C_p \tag{6}$$

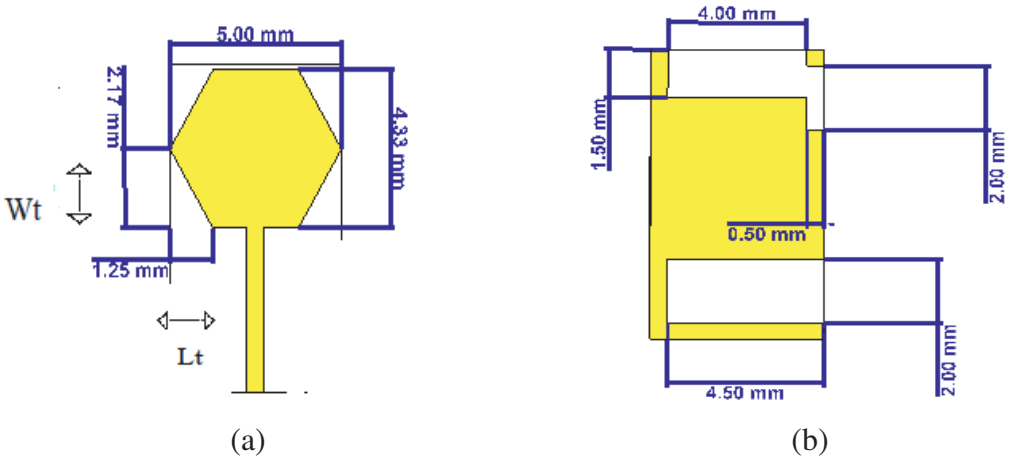

(a) (b)

Figure 9. Radiating element front and back views.

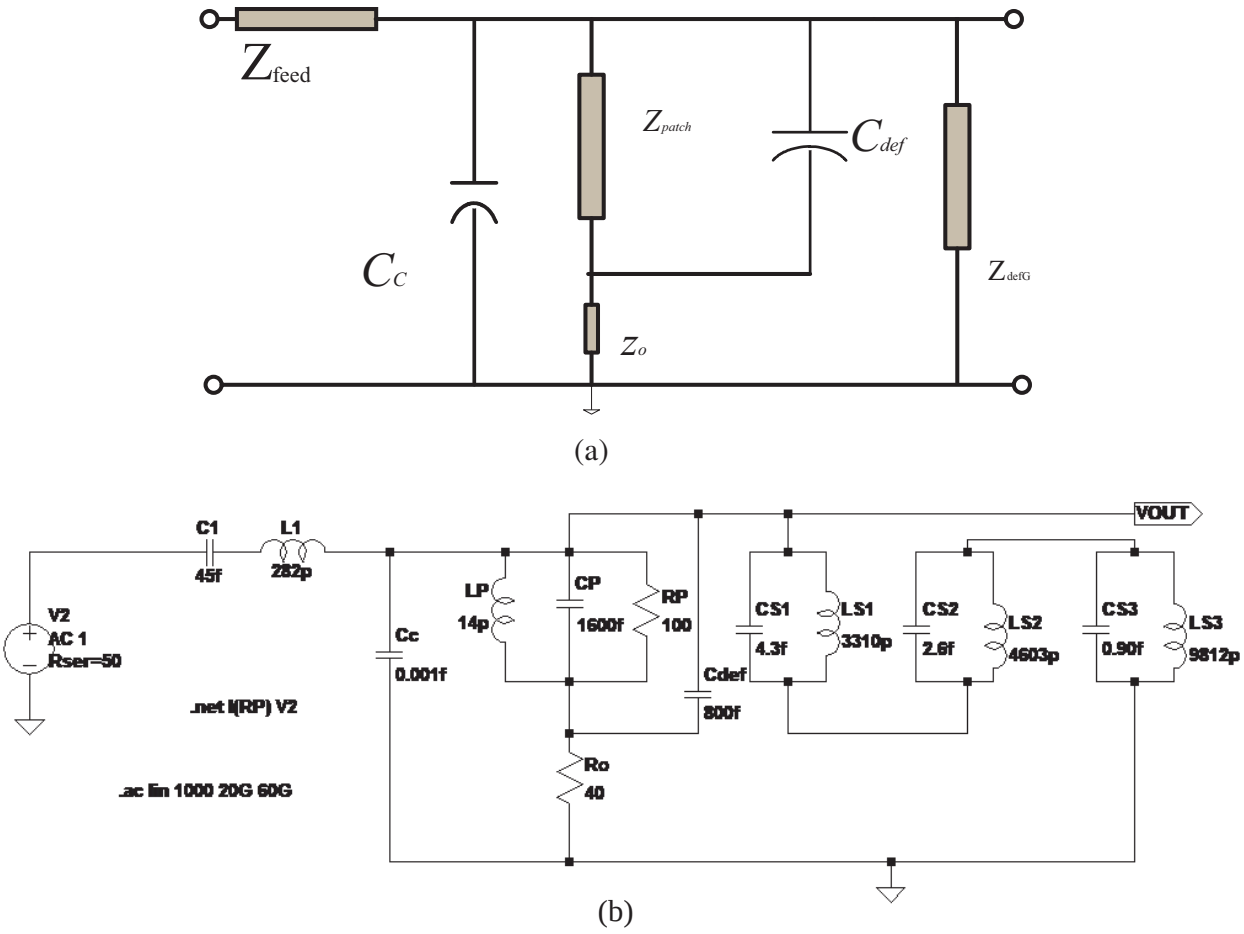

(a)

(b)

Figure 10. (a) Equivalent circuit of Hexagonal patch antenna with defected ground plane. (b) Simplified circuit model simulated using LTSPICE.

$$Q_r = c\sqrt{\in_{eff}}/hf_o \tag{7}$$

$$C_p = \frac{(\in_{eff} \in_o L_p W_p}{2h} \cos^{-2}\left(\frac{\pi Y_o}{L_p}\right) \tag{8}$$

$$L_p = 1/C_p(\omega_O^2) \tag{9}$$

$$S = 2 \times L_t \times W_t \tag{10}$$

$$C_{def} = (\varepsilon_o \varepsilon_{eff} S)/h \tag{11}$$

The simplified equivalent model is shown in Fig. 10(b). The simplified equivalent circuit includes capacitance C_1 and L_1 for feed. Cc is the coupling capacitance between the patch and feed. L_P, C_P, and R_P are related to usual patch impedance Z_P. C_{def} was derived from the conventional rectangular patch. The resistance Ro is added to compensate the effect of cutting triangular edges from the patch. The LC resonator circuits in series are added for the rectangular notches cut from the ground plane representing the impedance $ZdefG$.

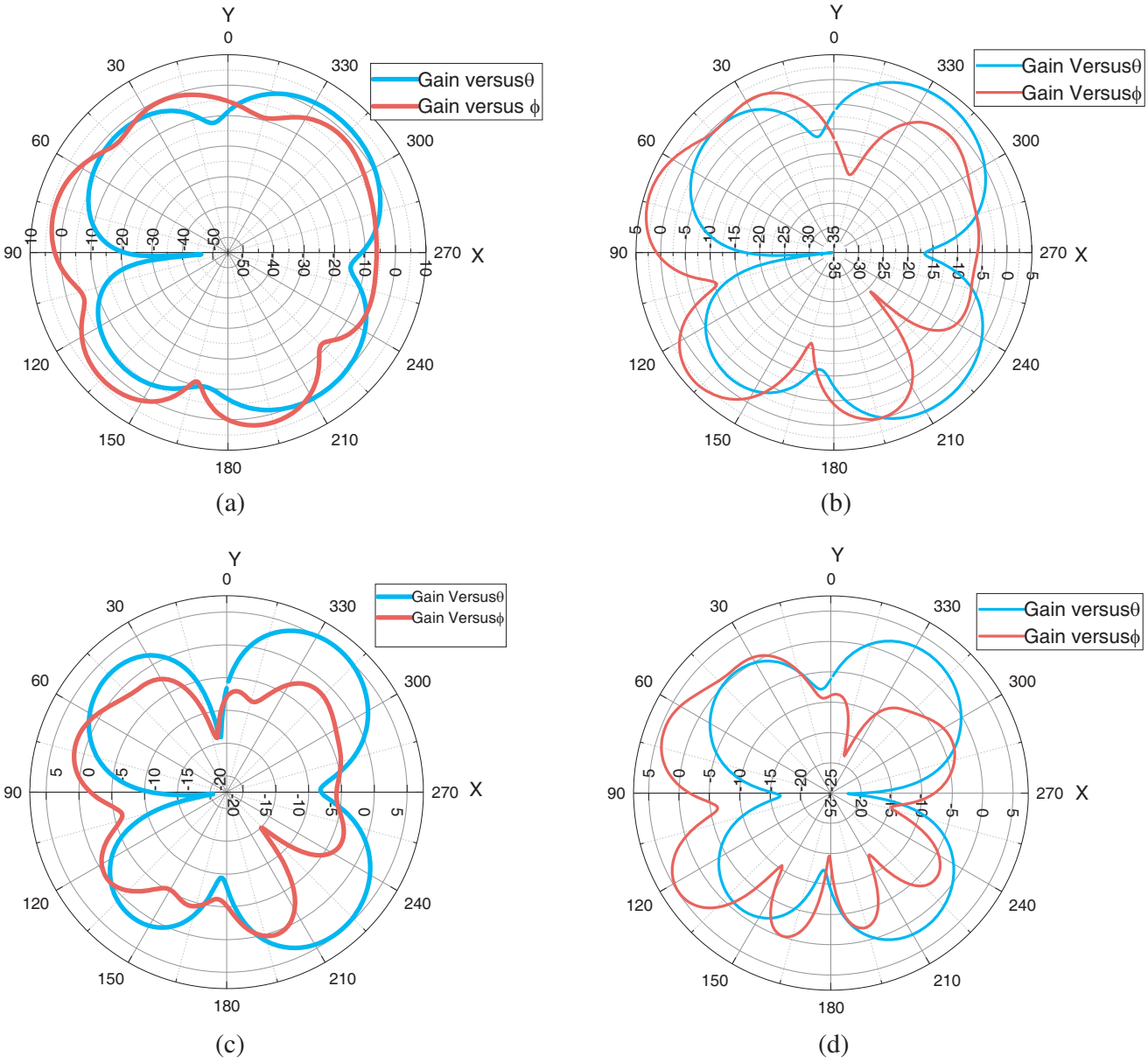

Figure 11. Simulated E and H plane patterns. (a) E and H plane pattern at 44 GHz. (b) E and H plane pattern at 45 GHz. (c) E and H plane pattern at 46 GHz. (d) E and H plane pattern at 52 GHz.

5. RADIATION PATTERNS

The gain variations along *E plane and H plane* are shown in Figs. 11(a), (b), (c), and (d) at 44 GHz, 45 GHz 46 GHz, and 52 GHz, respectively. The E plane pattern spans a main lobe at 321° and 324°, 324° and 325° with a half power width 48.7°, 47.4°, 33°, and 45°, respectively. The side lobe levels of −4.9 dB, −0.6 dB, −0.7 dB, and −1 dB are observed at 44 GHz, 45 GHz 46 GHz, and 52 GHz, respectively.

The angular half power beamwidth in the H plane is 33.4° at center frequency. Main lobe spans an angle from 216° to 325° over the band from 40 GHz to 52 GHz with average angular beamwidth of 47.5° along the θ plane and 31.45° in the ϕ plane. The main lobe magnitude varies from 6.22 dBi to 2.97 dBi with an average side lobe magnitude of −2.475 dB in θ plane.

6. S PARAMETERS (IMPEDANCE VIEW)

The normalized impedance chart is shown in Fig. 12. It is observed that at lower frequency 40 GHz of the resonant band (40 GHz–52 GHz), the impedance is inductive and slowly maps to resistive impedance at 44 GHz by adding capacitance in series moving in anticlockwise direction.

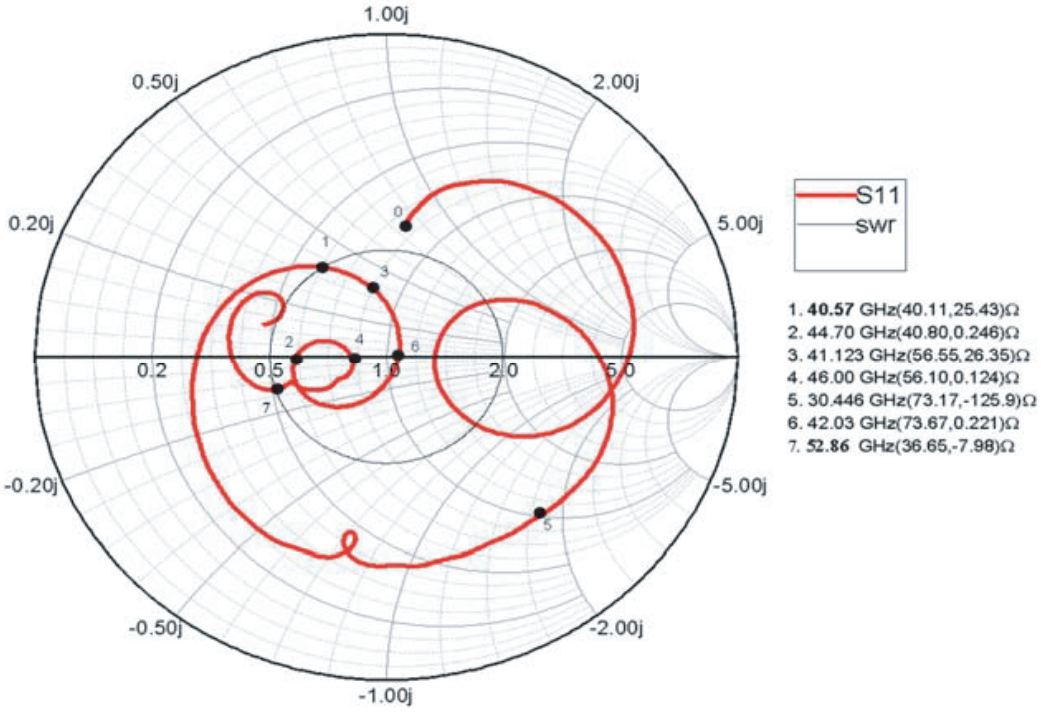

Figure 12. Simulated antenna impedance matching using Smith chart.

Similarly at 41.123 GHz impedance is inductive and maps to resistive impedance at 46.00 GHz. The impedance which was capacitive at 30 GHz maps to resistive impedance at 42 GHz moving in clockwise direction. Thus, impedance is resistive as shown with markers at 2, 4, and 6. The resonance is observed at 44.70 GHz, 46.00 GHz, and 42.03 GHz. These frequencies (40–52) GHz appear inside the VSWR circle of 1.99 thus approaching the band of resonance.

7. SURFACE CURRENT DISTRIBUTION

Figure 13(a) shows surface current distribution at 42 GHz. The current distribution is unidirectional with maximum current along the surface of the hexagon with 314.542 A/m.

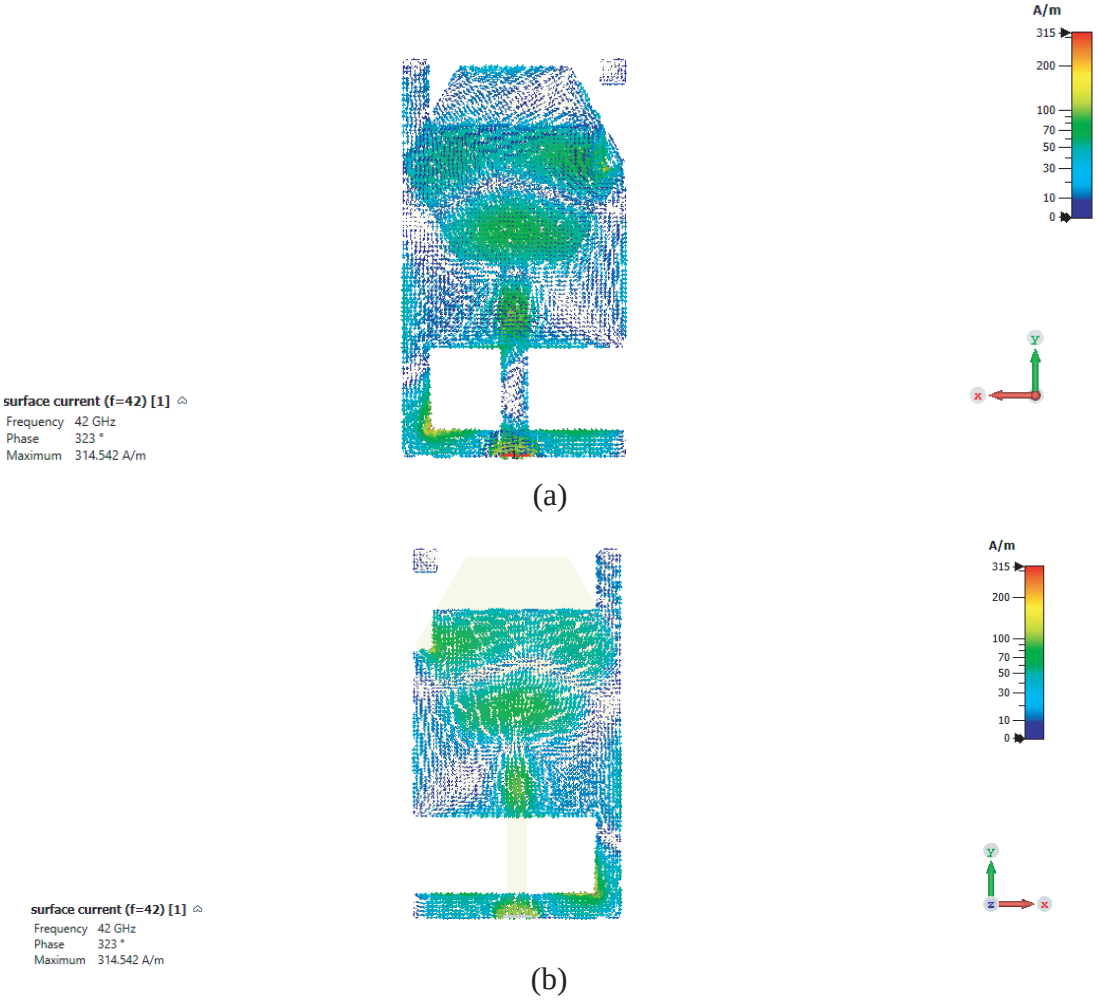

Figure 13. (a) Surface current distribution at 42 GHz front view. (b) Surface current distribution at 42 GHz ground view.

Figure 13(b) shows surface current distribution with maximum current distribution of along the surface in the back view also with a maximum current of 314.542 A/m.

8. FABRICATION AND TESTING

The proposed antenna has been fabricated using CVD technique and tested for frequencies ranging from 20 GHz to 60 GHz using VNA Details: Agilent N5247A: A.09.90.02. Through-Reflect-Line (TRL)

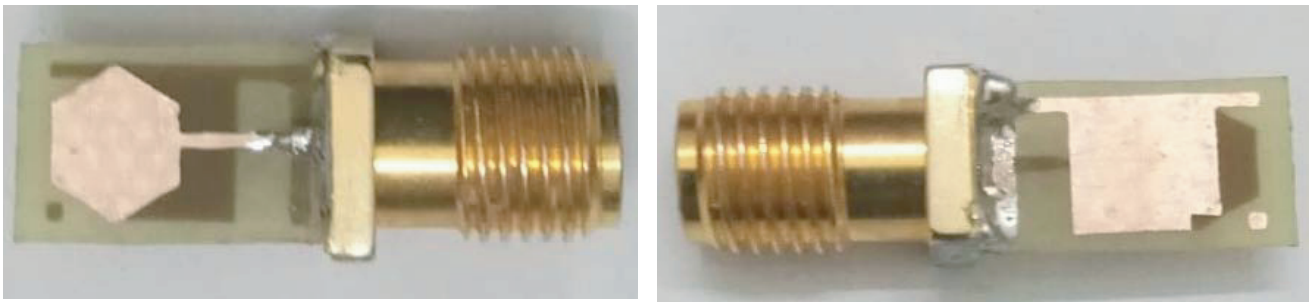

Figure 14. Fabricated antenna top and bottom views.

Figure 15. Measurement setup and results for VSWR parameter of the fabricated antenna.

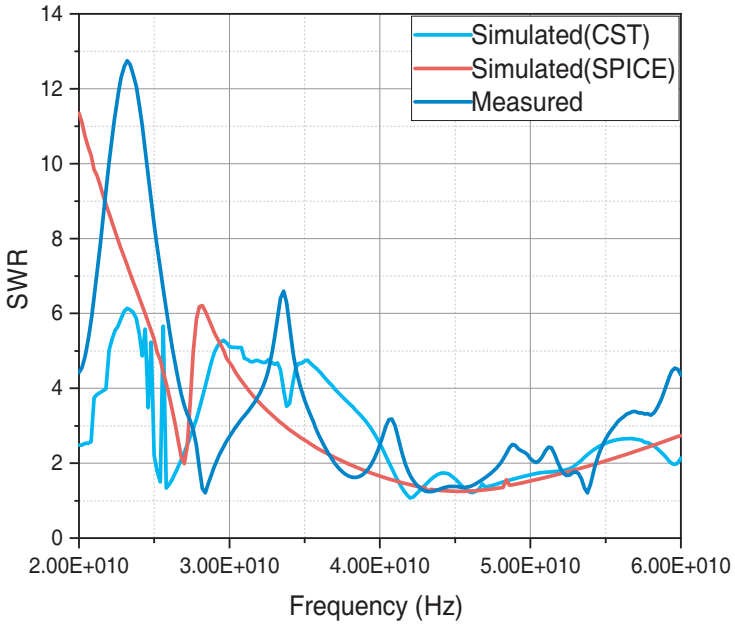

Figure 16. VSWR plot of CST simulated, SPICE simulated, and tested hexagonal patch antennas.

technique is used to calibrate the VNA with 3.5 SMA calibration kits. The top and bottom views of the fabricated antenna are shown in Fig. 14. The antenna has a dimension of $9 \times 5 \times 0.25\,\text{mm}^3$.

The measurement setup is shown in Fig. 15.

The VSWRs of the CST and SPICE simulated antennas and the tested antenna are shown in Fig. 16 where the fractional bandwidth is found to be 26% when being simulated using CST and 33% bandwidth when being simulated using SPICE whereas the tested antenna has a fractional bandwidth of 15% with resonance at 43 GHz. The deviation in measured and simulated results might be because of fabrication tolerances.

The gain plots of simulated and tested hexagonal antennas are shown in Fig. 17. The gain of simulated antenna is 5.3 dB to 6.5 dB over the band of 40 GHz to 52 GHz whereas the gain of tested

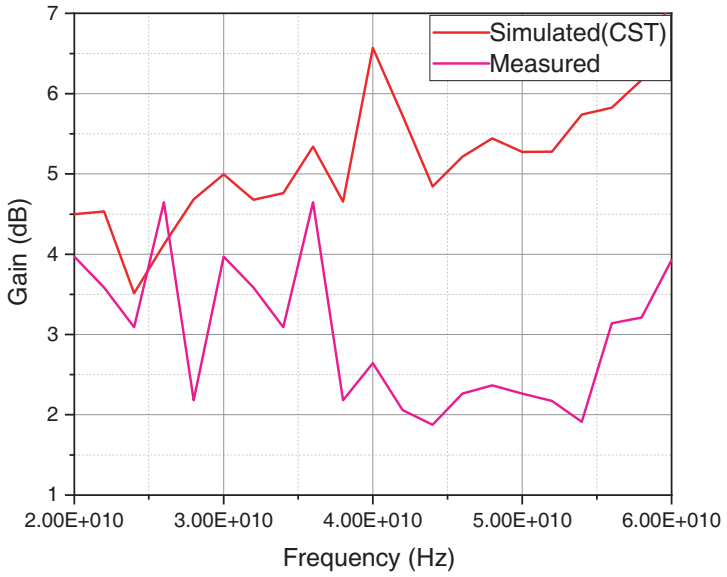

Figure 17. Gain of (CST) simulated and tested antennas.

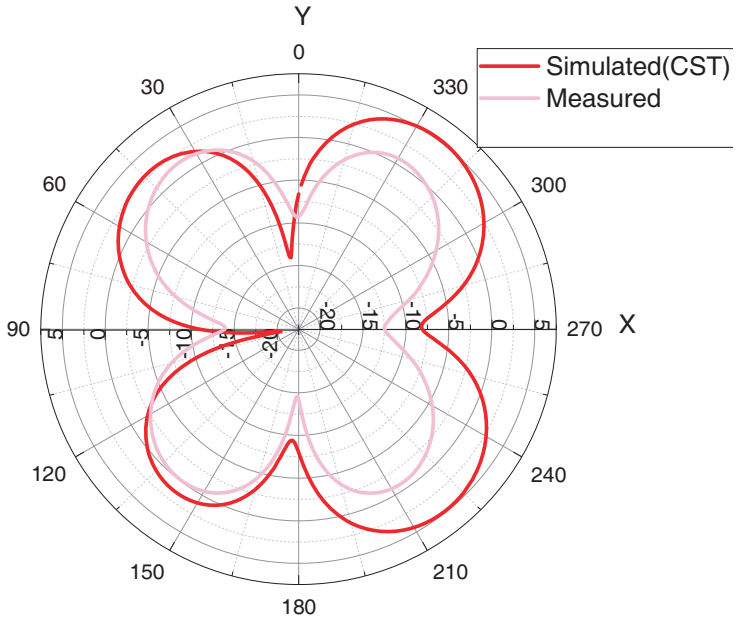

Figure 18. E plane of simulated (CST) and tested antennas at 46 GHz.

antenna varies from 2.3 dB to 2.5 dB over the band.

E plane patterns of simulated and tested antennas at a centre frequency of 46 GHz are shown in Fig. 18. The patterns show a nice similarity.

9. CONCLUSION

A low-profile millimeter wave antenna is designed for an ultra-wideband of 40–52 GHz with an effective percentage bandwidth of 26%. The hexagonal antenna with the dimension of 2.5 mm with defected ground plane is proposed. The proposed antenna is compared with planar mm-wave antennas existing in literature and is found to have optimum gain and efficiency in terms of size constraint. The hexagonal antenna is compared with circular patch antenna having the same optimized ground plane, and the results are tabulated. The antenna is designed to resonate at 42 GHz. The characteristic behavior of the antenna has been studied, and the results are presented. The equivalent circuit for the hexagonal antenna is derived and simulated using LT spice. The simulated radiation patterns of E plane and H plane are analyzed and are observed to have average low side-lobe level of -2.9 dB. The impedance parameters are also analyzed using Smith chart, and resonance is observed at designed frequency 42 GHz of the proposed hexagonal patch antenna. The antenna is fabricated, and tested results are matching with the simulated ones. Antennas size constraint enables integration and can be used in applications such as fixed and mobile satellite, earth explorations satellite, space research services, broadcasting satellite services, international mobile telecommunication services, and HAPS services in mm-wave domain.

ACKNOWLEDGMENT

We are thankful to management of NMAMIT, Nitte, for permitting us to take up research and allow us to use the lab facilities of department of Electronics and Communication.

REFERENCES

1. Al-Alem, Y. and A. A. Kishk, "Efficient millimeter-wave antenna based on the exploitation of microstrip line discontinuity radiation," *IEEE Transactions on Antennas and Propagation*, Vol. 66, No. 6, 2844–2852, 2018.
2. Dangi, R., P. Lalwani, G. Choudhary, I. You, and G. Pau, "Study and investigation on 5G technology: A systematic review," *Sensors*, Vol. 22, No. 1, 26, 2022.
3. Gupta, A. K. and A. Banerjee, *Spectrum above Radio Bands Spectrum Sharing: The Next Frontier in Wireless Networks*, 7596, 2020.
4. Itu, J., "Provisional final acts," *World Radiocommunication Conference 2019*, ITU Publications, 2019.
5. Martin, M. A., "Review on millimeter wave antennas-potential candidate for 5G enabled applications," *Advanced Electromagnetics*, Vol. 5, No. 3, 98, 2016.
6. Huang, J., C. H. Wang, R. Feng, J. Sun, W. Zhang, and Y. Yang, "Multi-frequency mmWave massive MIMO channel measurements and characterization for 5G wireless communication systems," *IEEE Journal on Selected Areas in Communications*, Vol. 35, No. 7, 1591–1605, 2017.
7. Li, Y. and J. Wang, "Dual-band leaky-wave antenna based on dual-mode composite microstrip line for microwave and millimeter-wave applications," *IEEE Transactions on Antennas and Propagation*, Vol. 66, No. 4, 1660–1668, 2018.
8. Anjos, E. V. P., D. M. M.-P. Schreurs, G. A. E. Vandenbosch, and M. Geurts, "A 14–50-GHz phase shifter with all-pass networks for 5G mobile applications," *IEEE Transactions on Microwave Theory and Techniques*, Vol. 68, No. 2, 762–774, 2019.
9. Huang, J., C. X. Wang, H. Chang, J. Sun, and X. Gao, "Multi-frequency multi-scenario millimeter wave MIMO channel measurements and modeling for B5G wireless communication systems," *IEEE Journal on Selected Areas in Communications*, Vol. 38, No. 9, 2010–2025, 2020.

10. Tripathi, S., N. V. Sab, K. G. Abhishek, and H. S. Dhillon, "Millimeter-wave and terahertz spectrum for 6G wireless," 6G Mobile Wireless Networks Cham, 83–121, Springer International Publishing, 2021.
11. Harini, V., M. V. S. Sairam, and R. Madhu, "A wide band log periodic millimeter-wave antenna for 5G femtocells applications," *Transactions on Emerging Telecommunications Technologies*, Vol. 32, No. 11, 2021.
12. Juneja, S., R. Pratap, and R. Sharma, "Semiconductor technologies for 5G implementation at millimeter wave frequencies — Design challenges and current state of work," *International Journal of Engineering Science and Technology*, Vol. 24, No. 1, 205–217, 2021.
13. Serrano, A. L. C., M. Gustavo, I. Abe, A. G. Palomino, and G. Rehder, "Millimeter-wave wireless integrated systems: What to expect for future solutions," *Journal of Integrated Circuits and Systems*, Vol. 17, No. 2, 1–7, 2022.
14. Farooq, U. and G. M. Rather, "A miniaturized Ka/V dual band millimeter wave antenna for 5G body centric network applications," *Alexandria Engineering J.*, Vol. 61, No. 10, 8089–8096, 2022.
15. Abbas, M. A., A. Allam, A. Gaafar, H. M. Elhennawy, and M. F. A. Sree, "Compact UWB MIMO antenna for 5G millimeter-wave applications," *Sensors*, Vol. 23, No. 5, 2702, 2023.
16. Ullah, H., H. F. Abutarboush, A. Rashid, and F. A. Tahir, "A compact low-profile antenna for millimeter-wave 5G mobile phones," *Electronics*, Vol. 11, No. 19, 3256, 2022.
17. Li, S., T. Chi, Y. Wang, and H. Wang, "A millimeter-wave dual-feed square loop antenna for 5G communications," *IEEE Transactions on Antennas and Propagation*, Vol. 65, No. 12, 6317–6328, IEEE, 2017.
18. Marzouk, H. M., M. I. Ahmed, and A. H. A. Shaalan, "Novel dual-band 28/38 GHz MIMO antennas for 5G mobile applications," *Progress In Electromagnetics Research C*, Vol. 93, 103–117, 2019.
19. Mahmoud, K. R. and M. M. Ahmed, "Performance of tri-band multi-polarized array antenna for 5G mobile base station adopting polarization and directivity control," *IEEE Access*, Vol. 6, 8682–8694, 2018.
20. Haraz, O. M., M. M. A. Mohamed, A. Saleh, and Abdel-R S. "Design of a 28/38 GHz dualband printed slot antenna for the future 5G mobile communication Networks," *2015 IEEE International Symposium on Antennas and Propagation & USNC/URSI National Radio Science Meeting*, 1532–1533, IEEE, 2015.
21. Kornprobst, J., K. Wang, G. Hamberger, and T. F. Eibert, "A mm-wave patch antenna with broad bandwidth and a wide angular range," *IEEE Transactions on Antennas and Propagation*, Vol. 65, No. 8, 4293–4298, 2017.
22. Hasan, M. N., S. Bashir, and S. Chu, "Dual band omnidirectional millimeter wave antenna for 5G communications," *J. of Electromagnetic Waves and Applications*, Vol. 33, No. 12, 1581–1590, 2019.
23. Wu, Q., J. Yin, C. Yu, H. Wang, and W. Hong, "Low-profile millimeter-wave SIW cavity backed dualband circularly polarized antenna," *IEEE Transactions on Antennas and Propagation*, Vol. 65, No. 12, 7310–7315, 2017.
24. Chu, Q.-X., X.-R. Li, and M. Ye, "High-gain printed log-periodic dipole array antenna with parasitic cell for 5G communication," *IEEE Transactions on Antennas and Propagation*, Vol. 65, No. 12, 6338–6344, 2017.
25. Agarwal, M., J. K. Dhanoa, and M. K. Khandelwal, "Two-port hexagon shaped MIMO microstrip antenna for UWB applications integrated with double stop bands for WiMax and WLAN," *AEU — International Journal of Electronics and Communications*, Vol. 138, 153885, 2021.
26. Vahid Sarani, A. and M. H. Neshati, "Design investigation of dual-band dual-circularly polarized hybrid antenna array using semi-hexagonal HMSIW cavity," *AEU — International Journal of Electronics and Communications*, Vol. 157, 154437, 2022.
27. Bahl, I. J. and P. Bartia, *Microstrip Patch Antenna*, Artech House, Massachusetts 02026, 1980.
28. Ez-zaki, F., A. B. Khaoula, S. Ahmad, H. Belahrach, A. Ghammaz, A. J. A. Al-Gburi, and O. P. Nasser, "Circuit modeling of broadband antenna using vector fitting and fostering form approaches for IoT applications," *Electronics*, Vol. 11, No. 22, 3724, 2022.